Electronic Supplementary information for:

The Role of Symmetric functionalisation on Photoisomerisation of a UV Commercial Chemical Filter.

Jack M. Woolley [a], Jack S. Peters [a], Matthew A. P. Turner [a,b], Guy J. Clarkson [a], Michael D. Horbury [a]*, and Vasilios G. Stavros.[a]*

[a.] Department of Chemistry, University of Warwick, Gibbet Hill Road, Coventry, CV4 7AL, UK.

[b.] Department of Physics, University of Warwick, Gibbet Hill Road, Coventry, CV4 7AL, UK

E-mail: v.stavros@warwick.ac.uk, m.horbury@warwick.ac.uk

1. NMR Data

All NMR measurements were conducted in deuterated chloroform at 400 MHz.

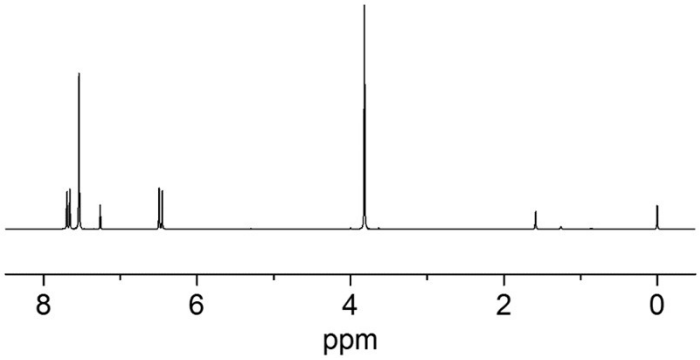

Figure S1. Full ^{1}H NMR of *E,E*-**DPD**. 7.68 ppm (d, 2H, J = 16.0 Hz, olefin), 7.54 ppm (s, 4H, phenylene), 6.48 ppm (d, 2H, J = 16.0 Hz, olefin) and 3.82 ppm (s, 6H, OMe).

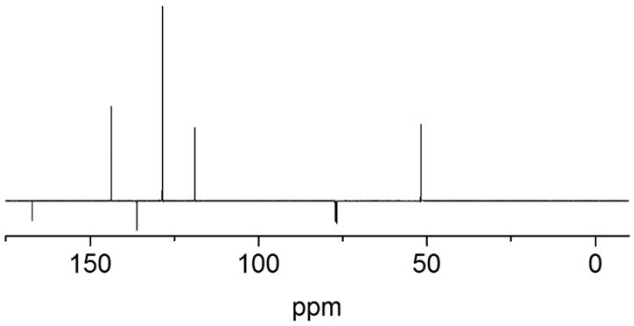

Figure S2. Full ^{13}C NMR of *E,E*-**DPD**. 167.2 ppm (COO), 143.7 ppm (olefin), 136.1 ppm (quaternary phenyl), 128.6 ppm (phenylene), 119.0 ppm (olefin) and 52.0 ppm (OMe).

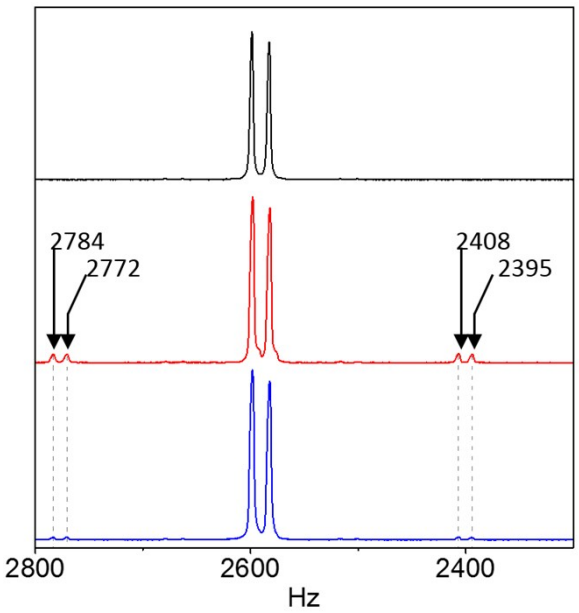

Figure S3. Region of ^{1}H NMR of *E,E*-**DPD**, showing the splitting of Z peaks post-irradiation in ethanol and acetonitrile, blue and red respectively. Black trace shows ^{1}H NMR pre-irradiation.

2. Crystallographic Data

Crystals were grown from DCM/petrol. A suitable crystal was selected and mounted on a glass fibre with Fomblin oil and placed on a Rigaku Oxford Diffraction SuperNova diffractometer with a duel source (Cu at zero) equipped with an AtlasS2 CCD area detector. The crystal was kept at 150(2) K during data collection. Using Olex2,[1] the structure was solved with the ShelXT[2] structure solution program using Intrinsic Phasing and refined with the ShelXL[3] refinement package using Least Squares minimisation. Data is deposited within the Cambridge Crystallographic Data base (CCDC

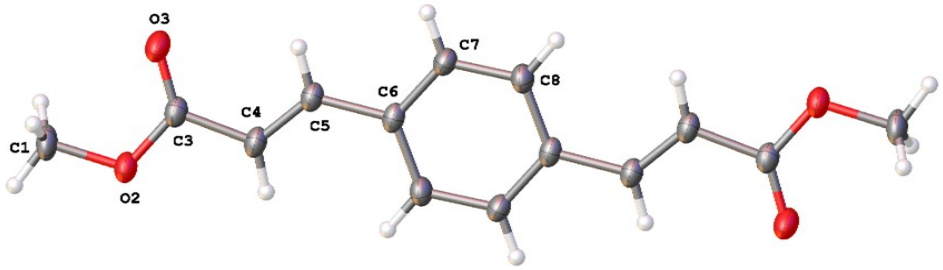

Figure S4. Molecular structure of *E,E*-**DPD** with only the atoms of the asymmetric unit labelled and thermal ellipsoids drawn at 50% probability.

1870247).

There is half a molecule in the asymmetric unit as the molecule sits on a crystallographic inversion centre in the middle of the phenyl ring. There is an entire molecule in the unit cell. The molecule has the *E* stereochemistry at either double bond.[4]

Table S1: Bond Lengths for *E,E*-**DPD**.

Atom	Atom	Length (Å)		Atom	Atom	Length (Å)
O2	C3	1.3421(15)		C6	C8[1]	1.3978(16)
O2	C1	1.4393(14)		C7	C8	1.3856(16)
O3	C3	1.2088(15)		C3	C4	1.4803(15)
C6	C7	1.3970(16)		C5	C4	1.3322(17)
C6	C5	1.4691(15)		C8	C6[1]	1.3978(16)

[1]2-X,2-Y,1-Z

Table S2: Bond Angles for *E,E*-**DPD**.

Atom	Atom	Atom	Angle (°)	Atom	Atom	Atom	Angle (°)
C3	O2	C1	114.43(9)	O3	C3	O2	123.18(10)
C7	C6	C5	118.75(10)	O3	C3	C4	125.42(11)
C7	C6	C8[1]	118.36(10)	C4	C5	C6	126.91(11)
C8[1]	C6	C5	122.88(11)	C5	C4	C3	119.52(11)
C8	C7	C6	120.98(11)	C7	C8	C6[1]	120.65(11)
O2	C3	C4	111.40(10)				

[1]2-X,2-Y,1-Z

3. Calculations

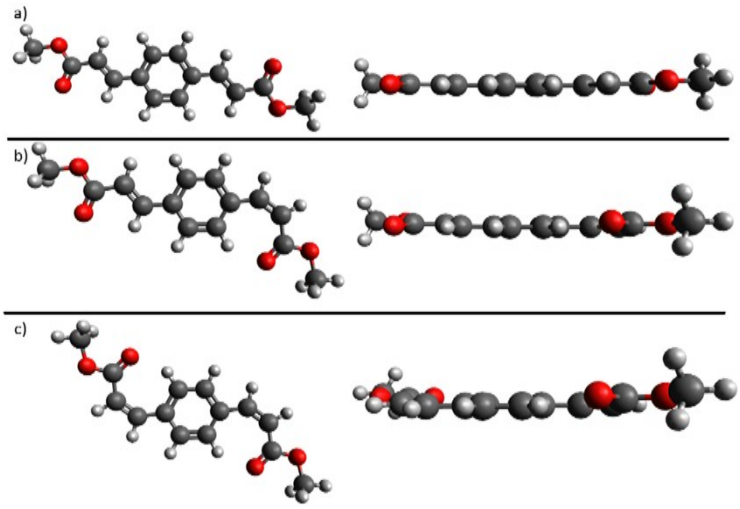

Figure S5. Calculated ground state molecular structures for all three geometric isomers shown both top-down and side-on. a) *E,E*-**DPD**, b) *E,Z*-**DPD** and c) *Z,Z*-**DPD**.

Table S3: Energies of the three possible isomers of **DPD**, relative to the energy of *E,E*-**DPD**, along with first singlet (vertical) excitation energies and their oscillator strengths, in acetonitrile, ethanol and cyclohexane.

Solvent	Isomer	*E,E*	*E,Z*	*Z,Z*
acetonitrile	ground state difference relative to *E,E*-**DPD** (eV)	0	0.27	0.54
	Vertical excitation energies eV (nm)	3.79 (327)	3.80 (326)	3.81 (325)
	Transition oscillator Strength	1.30	1.17	1.08
ethanol	ground state difference relative to *E,E*-**DPD** (eV)	0	0.27	0.55
	Vertical excitation energies eV (nm)	3.76 (330)	3.80 (326)	3.81 (325)
	Transition oscillator Strength	1.31	0.94	0.80
cyclohexane	ground state difference relative to *E,E*-**DPD** (eV)	0	0.35	0.58
	Vertical excitation energies eV (nm)	3.80 (326)	3.81 (325)	3.81 (325)
	Transition oscillator Strength	1.28	1.16	1.06

4. Additional TEAS Data

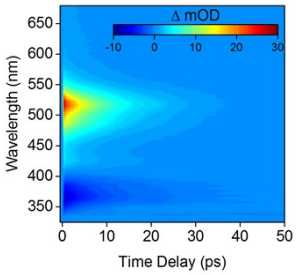

Figure S6. False colour heat map of *E,E*-**DPD** following photoexcitation at 317 nm in acetonitrile with the full intensity scale included (*cf.* Figure 2a in the main manuscript has its intensity scale cropped for visual purposes).

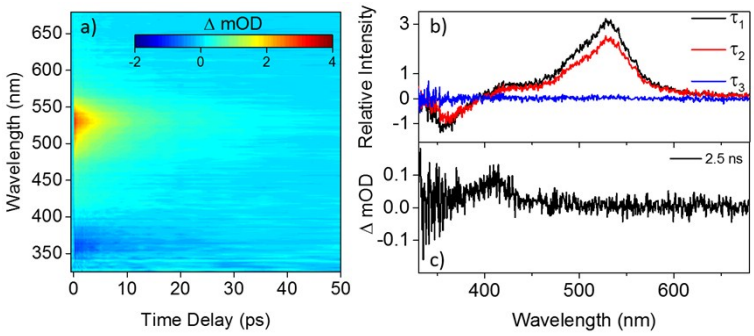

Figure S7. False colour heat maps of *E,E*-**DPD** following photoexcitation at 315 nm in a) cyclohexane. b) Evolutionary associated difference spectra for the TAS of *E,E*-**DPD** in cyclohexane. c) TAS at Δt = 2.5 ns of *E,E*-**DPD** in cyclohexane.

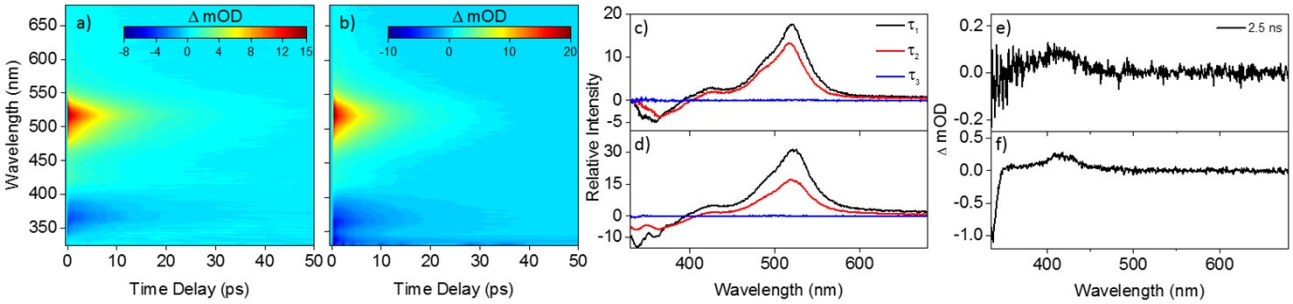

Figure S8. False colour heat maps of *E,E*-**DPD** following photoexcitation at a) 327 nm in acetonitrile and b) 329 nm in ethanol. Evolutionary associated difference spectra (EADS) for the TAS of *E,E*-**DPD** in c) acetonitrile and d) ethanol. TAS at Δt = 2.5 ns of *E,E*-**DPD** in e) acetonitrile and f) ethanol.

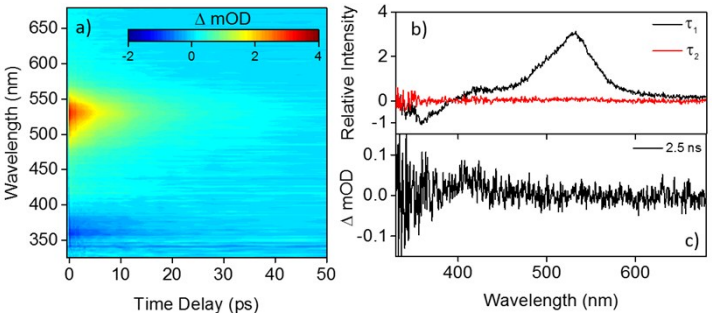

Figure S9. False colour heat maps of *E,E*-**DPD** following photoexcitation at a) 329 nm in cyclohexane. b) Evolutionary associated difference spectra (EADS) for the TAS of *E,E*-**DPD** in cyclohexane. C) TAS at Δt = 2.5 ns of *E,E*-**DPD** in cyclohexane.

Table S4. Lifetimes and associated errors (2σ) extracted from the global sequential fitting of *E,E*-**DPD,** following Photoexcitation at 327 nm for acetonitrile, and 329 nm for both ethanol and cyclohexane.

Solvent	τ_1 (fs)	τ_2 (ps)	τ_3 (ns)
E,E-**DPD**			
acetonitrile	190 ± 40	8.70 ± 0.04	>>2.5
ethanol	190 ± 40	7.82 ± 0.04	>>2.5
cyclohexane	-	10.08 ± 0.10	>>2.5

5. Transient Slices of Key Features

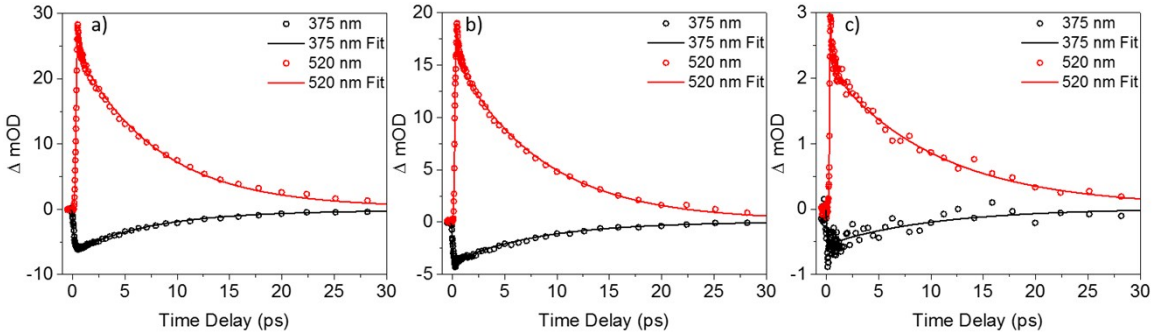

Figure S10. Single wavelength transient slices of *E,E*-**DPD**, taken for the stimulated emission (375 nm) and excited state absorption (520 nm) features following photoexcitation at a) 317 nm in acetonitrile, b) 318 nm in ethanol and c) 315 nm in cyclohexane. Solid lines indicate the extracted fit from the sequantial model (see main manuscript). The comparison serves to demonstrate the quality of the fit.

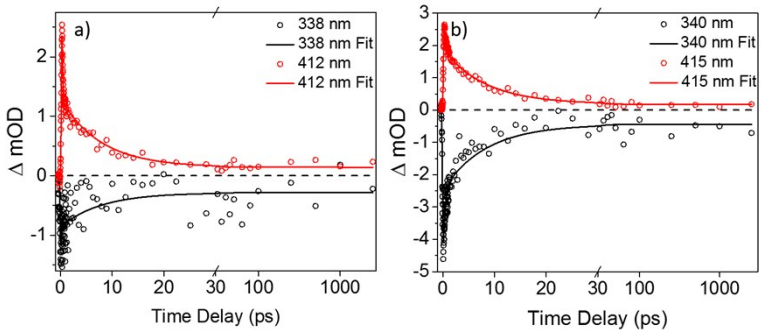

Figure S11. Single wavelength transient slices *E,E*-**DPD**, taken across the ground state bleach and excited state absorption of the $^1n\pi^*$ state following photoexcitation at a) 317 nm in acetonitrile and b) 318 nm in ethanol (signal-to-noise prohibits a similar analysis for cyclohexane). Solid lines indicate the extracted global sequential fit, at given wavelengths.

6. Residuals

The percentage difference for each data point between the experimental TAS and the calculated TAS was determined using Eqn. 1. These values were then averaged and given as a semi-quantitative guide for the quality of each residual.

$$percentage\ difference = \left| {X_{Exp} - X_{Fit}}/{X_{Fit}} \right| \times 100 \qquad \text{Equation 1}$$

Where X_{Exp}, corresponds to the measured value for each wavelength and time delay, and X_{Fit} corresponds to the calculated value for each wavelength and time delay.

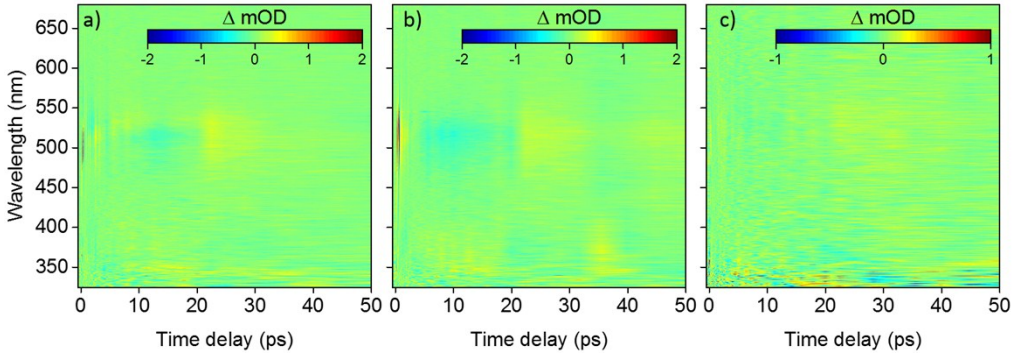

Figure S12. False colour heat maps of fitting residuals for *E,E*-**DPD** following photoexcitation at 317 nm, 318 nm and 315 nm in: in a) acetonitrile, b) ethanol and c) cyclohexane respectively. Average percentage errors for each residual was calculated to be 4.7%, 3.8% and 10% for acetonitrile, ethanol and cyclohexane respectively.

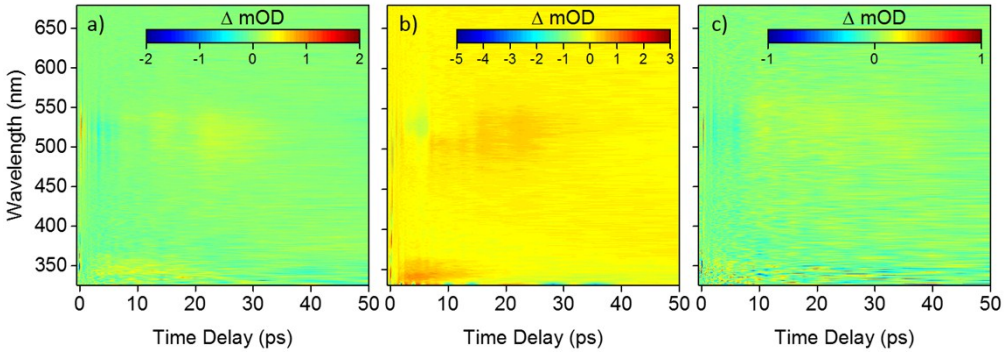

Figure S13. False colour heat maps of fitting residuals for *E,E*-**DPD** following photoexcitation at 327 nm, 329 nm and 329 nm in: in a) acetonitrile, b) ethanol and c) cyclohexane respectively. Average percentage errors for each residual was calculated to be 4.1%, 4% and 15% for acetonitrile, ethanol and cyclohexane respectively.

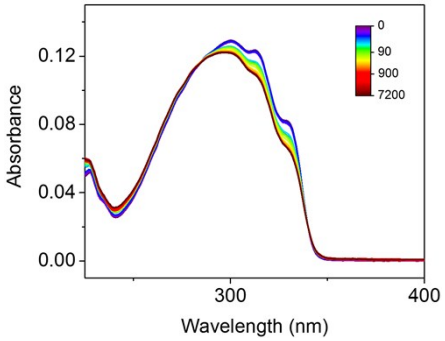

Figure S14. Steady-state UV/Vis absorption spectra of 10 µM *E,E*-**DPD** in cyclohexane, following irradiation at solar fluence over the corresponding peak absorption (λ_{max} = 315 nm; see Figure 1 main manuscript). Colour bar indicates length of irradiation in seconds.

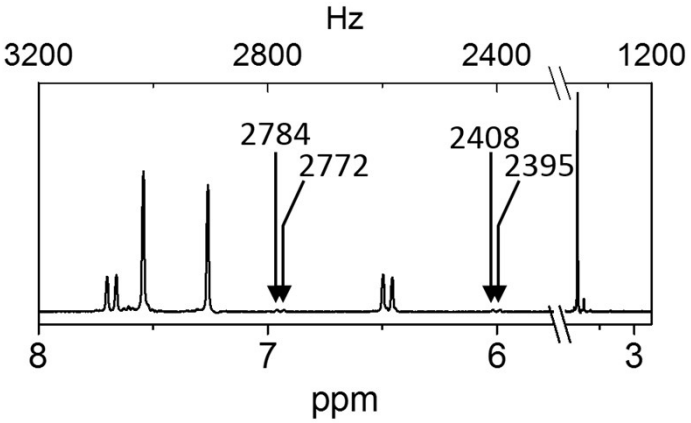

Figure S15. Region of ^{1}H NMR of *E,E*-**DPD** following irradiation in cyclohexane, showing the splitting of *Z* peaks following irradiation in cyclohexane.

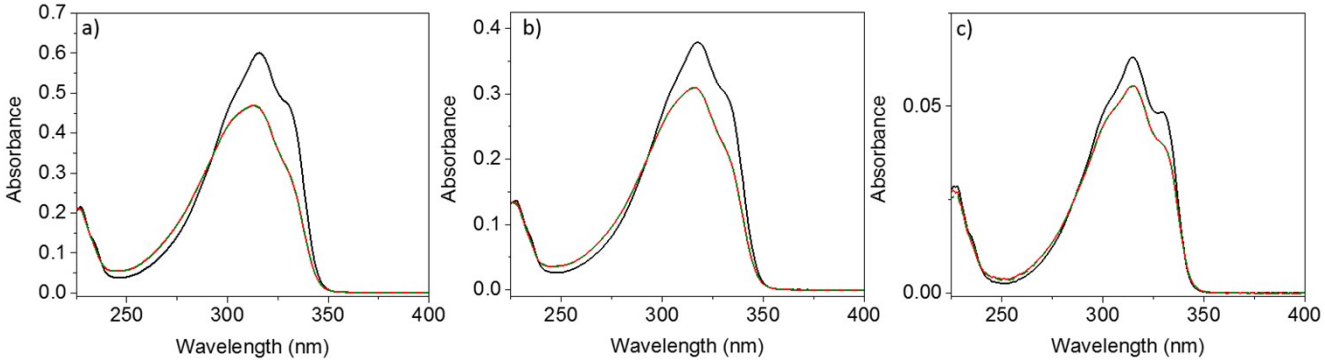

Figure S16. Steady-state UV/Vis absorption of 10 µM *E,E*-**DPD** in a) acetonitrile b) ethanol and <10 µM in c) cyclohexane. Black trace is pre-irradiation. Red trace is following 40 minutes of irradiation at solar fluence for each peak wavelength (317 nm, 318 nm and 315 nm, for acetonitrile ethanol and cyclohexane respectively). Dashed green trace is after leaving the post-irradiated sample stand (in darkness) for 2 hours.

7. Additional Steady-state Data

8. Fluorescence Quantum Yield

Fluorescence Quantum yields of *E,E*-**DPD**, were obtained through, equation 2,[5] with the use of diphenyl-1,3-butadiene (DPB) method as a reference (Φ_f = 0.44).[6] Five fluorescence sets were acquired and the standard deviation between them taken as the error.

$$\Phi_{f,\,DPD} = \Phi_{f,\,ref}{}^{F_{DPD}}\!/_{F_{ref}} \cdot {}^{f_{ref}}\!/_{f_{DPD}} \cdot {}^{n_{DPD}^2}\!/_{n_{ref}^2} \qquad \text{Equation 2}$$

where Φ_f is the fluorescence quantum yield, F is the integral photon flux and n is the refractive index at the wavelength corresponding to half the total integration of the fluorescence emission spectrum. $f = 1 - 10^{-A}$, where A is the aborbance at the excitation wavelength. The calculated fluorescence quantum yield of *E,E*-**DPD** is thus determined to

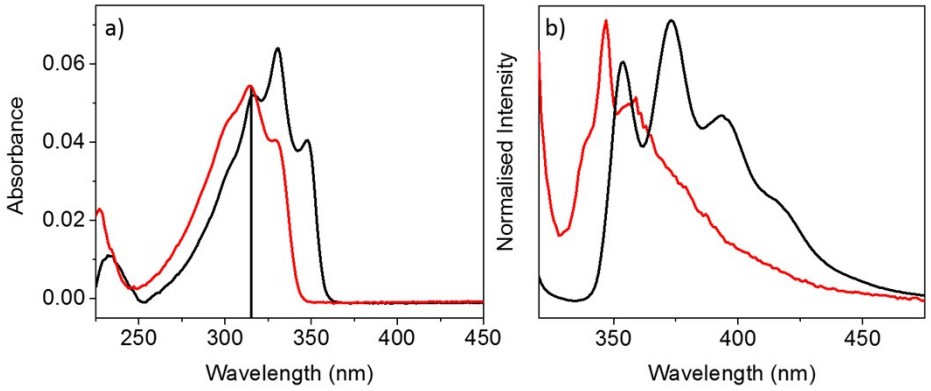

Figure S17. a) UV/Vis of both *E,E*-**DPD** and DPB in cyclohexane, red and black respectively, with the vertical line showing the fluorescence excitation. b) Fluorescence emission for both *E,E*-**DPD** and DPB in cyclohexane, red and black respectively.

be 0.039 ± 0.002.

9. Power Studies

Pump power dependencies of *E,E*-**DPD** show a linear dependence across the spectral features of the TAS. These measurements were achieved by varying the TOPAS output power and taking a 10 nm integration window across a particular spectral window at a given pump-probe (Δt) time delay. Each TAS displays a linear relationship to the incident pump power (log(signal) *vs.* log(power) plots), strongly suggesting single-photon induced dynamics.

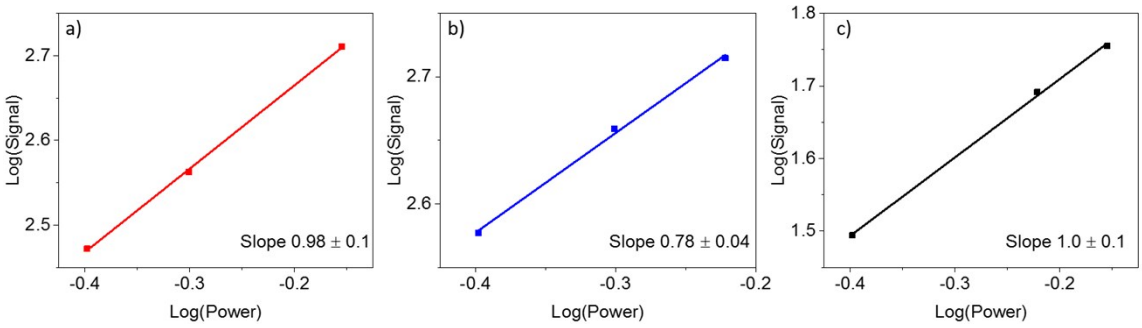

Figure S18. Power dependencies for the integrated intensity for *E,E*-**DPD** in: a) acetonitrile following excitation at 317 nm; 10 nm integration window, 515-525 nm, at Δt = 1 ps pump-probe delay. b) ethanol following excitation at 318 nm; 10 nm integration window, 515-525 nm, at Δt = 1 ps pump-probe delay. c) cyclohexane following excitation at 315 nm; 10 nm integration window, 515-525 nm, at Δt = 1 ps pump-probe delay.

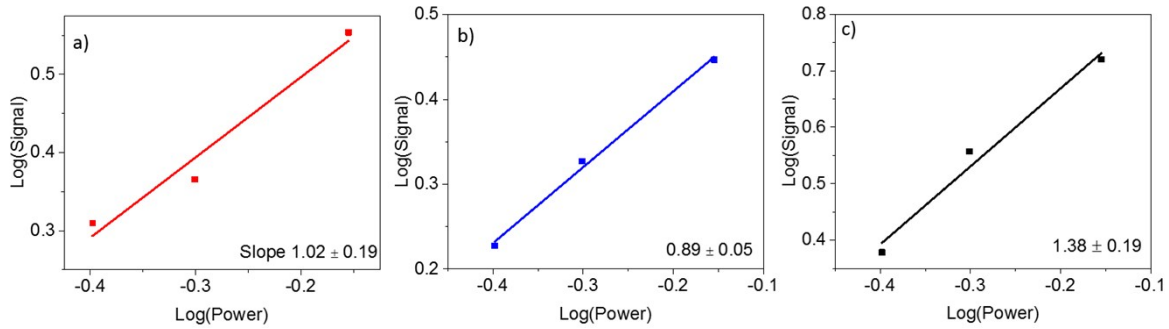

Figure S19. Power dependencies for the integrated intensity for *E,E*-**DPD** in: a) acetonitrile following excitation at 317 nm; 10 nm integration window, 405-415 nm, at Δ*t* = 2.5 ns pump-probe delay. b) ethanol following excitation at 318 nm; 10 nm integration window, 405-415 nm, at Δ*t* = 2.5 ns pump-probe delay. c) cyclohexane following excitation at 315 nm; 10 nm integration window, 405-415 nm, at Δ*t* = 2.5 ns pump-probe delay.

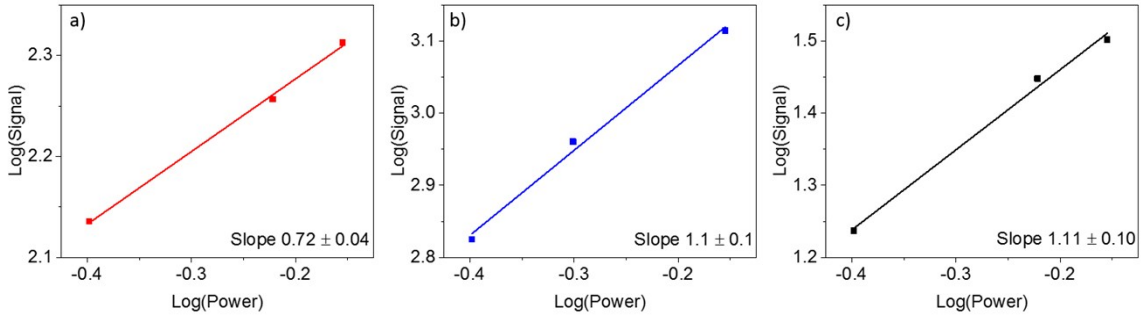

Figure S20. Power dependencies for the integrated intensity for *E,E*-**DPD** in: a) acetonitrile following excitation at 327 nm; 10 nm integration window, 515-525 nm, at Δ*t* = 1 ps pump-probe delay. b) ethanol following excitation at 329 nm; 10 nm integration window, 515-525 nm, at Δ*t* = 1 ps pump-probe delay. c) cyclohexane following excitation at 329 nm; 10 nm integration window, 515-525 nm, at Δ*t* = 1 ps pump-probe delay.

10. References

1 O. V. Dolomanov, L. J. Bourhis, R. J. Gildea, J. A. K. Howard and H. Puschmann, *J. Appl. Crystallogr.*, 2009, **42**, 339–341.

2 G. M. Sheldrick, *ActaCryst*, 2015, **A71**, 3–8.

3 G. M. Sheldrick, *Acta Crystallogr. Sect. C Struct. Chem.*, 2015, **C71**, 3–8.

4 K. Ueno, H. Nakanishi and M. Hasegawa, *Acta Crystallogr. Sect. B Struct. Sci. Cryst. Eng. Mater.*, 1978, **34**, 2034–2035.

5 C. Würth, M. Grabolle, J. Pauli, M. Spieles and U. Resch-Genger, *Nat. Protoc.*, 2013, **8**, 1535–1550.

6 K. Dahl, R. Biswas and M. Maroncelli, *J. Phys. Chem. B*, 2003, **107**, 7838–7853.